Acta Crystallographica Section D
Biological Crystallography
ISSN 1399-0047

Insights into the relationship between the haem-binding pocket and the redox potential of c_6 cytochromes: four atomic resolution structures of c_6 and c_6-like proteins from *Synechococcus* sp. PCC 7002

Wojciech Bialek,[a]‡ Szymon Krzywda,[b]‡ Pawel Zatwarnicki,[a] Mariusz Jaskolski,[b,c] Piotr Kolesinski[a] and Andrzej Szczepaniak[a]*

[a]Department of Biophysics, Faculty of Biotechnology, University of Wroclaw, Wroclaw, Poland, [b]Department of Crystallography, Faculty of Chemistry, A. Mickiewicz University, Poznan, Poland, and [c]Center for Biocrystallographic Research, Institute of Bioorganic Chemistry, Polish Academy of Sciences, Poznan, Poland

‡ These authors contributed equally to this work.

Correspondence e-mail: aszczep@ibmb.uni.wroc.pl

Received 14 April 2014
Accepted 5 June 2014

PDB references: cytochrome c_6, 4eic; cytochrome c_6 Q57V, 4eid; cytochrome c_{6C}, 4eie; cytochrome c_{6C} L50Q, 4eif

The structure of cytochrome c_{6C} from the mesophilic cyanobacterium *Synechococcus* sp. PCC 7002 has been determined at 1.03 Å resolution. This is the first structural report on the recently discovered cyanobacterial cytochrome c_6-like proteins found in marine and nitrogen-fixing cyanobacteria. Despite high similarity in the overall three-dimensional fold between cytochromes c_6 and c_{6C}, the latter shows saliently different electrostatic properties in terms of surface charge distribution and dipole moments. Its midpoint redox potential is less than half of the value for typical c_6 cytochromes and results mainly from the substitution of one residue in the haem pocket. Here, high-resolution crystal structures of mutants of both cytochromes c_6 and c_{6C} are presented, and the impact of the mutation of specific residues in the haem-binding pocket on the redox potential is discussed. These findings contribute to the elucidation of the structure–function relationship of c_6-like cytochromes.

1. Introduction

A gene encoding the small, high-potential, monohaem protein cytochrome (cyt) c_6 is found in most cyanobacterial genomes sequenced to date. The protein is an electron donor to cyt *c* oxidase in the respiration process of cyanobacteria, but it also transfers an electron between cyt b_6f and photosystem I in cyanobacterial and algal photosynthesis. However, in some cyanobacteria and algae cyt c_6 can be replaced by the copper protein plastocyanin (PC), depending on copper availability in the medium. Interestingly, PC has absolutely replaced cyt c_6 in plants, although they contain a modified cyt c_6-like protein, cyt c_{6A}.

The annotated genome sequence of the mesophilic cyanobacterium *Synechococcus* sp. PCC 7002 revealed the presence of several genes for small cytochromes *c*, *i.e.* *petJ1* (A0167), *petJ2* (A2391), *cytM* (A0375) and *psbV* (A0112), encoding cyt c_6, a cyt c_6-like protein, cyt c_M and cyt c_{550}, respectively (accession codes in parentheses are from the STRING database; http://string-db.org). Whereas cyt c_6 is a well characterized protein and c_{550} is a component of the oxygen-evolving centre of photosystem II, the functions of the c_M and c_6-like proteins remain obscure. Using phylogenetic analyses, we have shown that the cyt c_6-like protein, tentatively named cyt c_{6C}, differs from algal and plant cyt c_{6A} (Bialek *et al.*, 2008). Moreover, we have identified yet another cluster of cyanobacterial cyt c_6-like proteins, namely cyt c_{6B} proteins, which are found exclusively in closely related species of the marine cyanobacteria *Synechococcus* and *Prochlorococcus*. In contrast, cyt c_{6C} mostly occurs in the genomes of heterocyst-

forming or unicellular nitrogen-fixing cyanobacteria, as well as in non-nitrogen-fixing species such as the well studied *Synechococcus* sp. PCC 7002. The properties of cyt c_{6C} and cyt c_6 from this cyanobacterium differ substantially (*e.g.* pI 9.7 and $E_{m,7}$ = +148 mV *versus* pI 3.8 and $E_{m,7}$ = +333 mV, respectively), implying that cyt c_{6C}, unlike plastocyanin, cannot readily replace cyt c_6 at the same stage of photosynthesis, *i.e.* in the electron-transfer reaction between the cyt b_6f complex and photosystem I (Bialek *et al.*, 2008). On the other hand, it has recently been shown that cyt c_{6C} from *Nostoc* sp. PCC 7119 can reduce photosystem I, although not as efficiently as cyt c_6 and plastocyanin (Reyes-Sosa *et al.*, 2011).

The structures of cyts c_6 from cyanobacteria (Beissinger *et al.*, 1998; Bialek *et al.*, 2009; Sawaya *et al.*, 2001; Worrall *et al.*, 2007), algae (Akazaki *et al.*, 2008; Dikiy *et al.*, 2002; Frazão *et al.*, 1995; Kerfeld *et al.*, 1995; Schnackenberg *et al.*, 1999; Yamada *et al.*, 2000) and a diatom (Akazaki *et al.*, 2009) have been determined, as has the structure of cyt c_{6A} from *Arabidopsis thaliana* (Chida *et al.*, 2006; Marcaida *et al.*, 2006). Despite their various origins and different biophysical properties (in the case of c_6 and c_{6A}), all of these proteins share several structural motifs typical of class I cyts *c*. In addition, an outer membrane *c*-type cyt, OmcF, from *Geobacter sulfurreducens*, a nonphotosynthetic, dissimilar metal-reducing organism, shares structural similarities with cyt c_6, whereas its redox properties are more like those of cyt c_{6A} and especially c_{6C} (Lukat *et al.*, 2008; Pokkuluri *et al.*, 2009). Here, we report the first three-dimensional structure of a cyanobacterial cyt c_6-like protein: cyt c_{6C} from *Synechococcus* sp. PCC 7002. To determine whether the differences in the haem-binding pocket of cyt c_6 and c_6-like proteins influence the properties of these proteins, we have also characterized variants with mutations of specific residues. Specifically, we present the high-resolution crystal structure of a mutated cyt c_{6C} in which a conservative leucine at position 50 has been substituted by glutamine, which is specific for c_6 cytochromes, and show that this mutation increases the redox potential by 48 mV. In addition, we have determined high-resolution structures of cyt c_6 from the same cyanobacterium and a mutant of cyt c_6 in which the glutamine at position 57 has been replaced with valine, as found at the corresponding position in the cyt c_6-like sequence. Our study presents a comparison of the overall structure, and especially of the haem pocket, of the two proteins.

2. Materials and methods

2.1. Site-directed mutagenesis

Mutations were introduced using the QuikChange Site-Directed Mutagenesis Kit (Stratagene). To generate the Q57V cyt c_6 and L50Q cyt c_{6C} mutants, the vectors pUCJ1 and pUCJ2 (Bialek *et al.*, 2008) were used, respectively, as templates. The incorporation of the correct mutations and the absence of undesired changes were confirmed by DNA sequencing.

2.2. Protein expression and purification

Escherichia coli strain DH5α was co-transformed with the pUCJ2 (Bialek *et al.*, 2008) and pEC86 plasmids carrying the genes for the proteins responsible for cytochrome maturation (Braun & Thöny-Meyer, 2004). The former harbours a gene encoding mature cyt c_{6C} from *Synechococcus* sp. PCC 7002, whereas the latter harbours the haem-maturation genes (Arslan *et al.*, 1998). 5 ml of overnight culture was used to inoculate 1.7 l TB medium in a 2 l flask. Cultures were grown for 8 h at 37°C with vigorous agitation and then for 72–96 h at 30°C with agitation at 55 rev min^{-1}. Cells were harvested at 6000*g* at 4°C and washed in a buffer consisting of 10 m*M* Tris pH 7.5, 0.1 *M* NaCl, 20% sucrose, 1 m*M* EDTA. After centrifugation and resuspension in the same buffer, the periplasmic proteins were released by treatment with lysozyme (0.2 mg ml^{-1}) at 4°C for 1 h with shaking and were then centrifuged at 25 000*g* for 15 min at 4°C. The supernatant, which contains the periplasmic protein fraction, was incubated with ammonium sulfate (45% saturation, 30 min, 4°C) and centrifuged at 20 000*g* for 20 min at 4°C. The pellet was discarded. Ammonium sulfate was added to the supernatant to 95% saturation and the treatment described above was repeated. The red pellet was resuspended in 20 m*M* Tris pH 8.0, 2 *M* ammonium sulfate, 1 m*M* PMSF and loaded onto a HiTrap Phenyl column (GE Healthcare) connected to an ÄKTApurifier system and equilibrated with the same buffer. Proteins were eluted using a decreased concentration of ammonium sulfate. Fractions collected from the first column run were dialyzed against 20 m*M* Tris pH 8.0, 0.1 *M* NaCl. After overnight dialysis, the sample was applied onto a HiTrap SP FF column (GE Healthcare) equilibrated with the same buffer. Proteins were eluted with a linear 100–500 m*M* NaCl gradient. Purified cyt c_{6C} was characterized by SDS–PAGE and haem staining as described in Bialek *et al.* (2008). The A_{555}/A_{280} ratio of purified cyt c_{6C} was 0.9. Cyt c_6 was purified as described in Bialek *et al.* (2009) and Q57V cyt c_6 was purified in the same way. The proteins were aliquoted and stored at −20 °C.

2.3. Cytochrome absorption spectroscopy, haem quantitation and redox titrations

All spectroscopic measurements were performed using a Beckman DU800 spectrophotometer. Measurements were taken at room temperature using a 1 cm path-length cuvette. Cytochromes were diluted to a final concentration of 5 μM in 10 m*M* Tris pH 7.5 containing 1 m*M* potassium ferricyanide (spectra of oxidized cytochromes) or 1 m*M* sodium dithionate (spectra of reduced cytochromes). Redox titrations were performed as described by Dutton (1978). Titrations were performed three times in both directions in a custom-made anaerobic cuvette, using a platinum electrode and a calomel reference electrode under an argon flow in 50 m*M* MOPS pH 7.0, 100 m*M* KCl in the presence of redox mediators: tetrachlorohydroquinone (TCHQ; $E_{m,7}$ = 350 mV), 2,3,5,6-tetramethyl-*p*-phenylenediamine (DAD; 260 mV), 1,2-naphthoquinone-4-sulfonate (NQS; 210 mV), 1,2-naphthoquinone

(NQ; 130 mV), phenazine methosulfate (PMS; 80 mV), phenazine ethosulfate (PES; 55 mV) and duroquinone (DQ; 5 mV). All redox mediators were at a concentration of 45 µ*M* and the cytochromes were at 5 µ*M* (c_6 and Q57V c_6) or 1 µ*M* (c_{6C} and L50Q c_{6C}). 50 m*M* potassium ferricyanide was used as an oxidant and 50 m*M* sodium dithionate was used as a reductant. Spectra were recorded over the range 400–600 nm in intervals of 10–30 mV. Midpoint potentials were obtained from the cytochrome α-band absorbance plotted against the corresponding voltage.

2.4. Protein crystallization

Screening tests for cytochrome c_6 and Q57V c_6 crystallization conditions were performed manually using Crystal Screen, Crystal Screen 2 and Structure Screen I and II (Hampton Research; Jancarik & Kim, 1991; Wooh *et al.*, 2003) using the hanging-drop vapour-diffusion technique at 292 K by mixing 1 µl protein solution (1 m*M* in 10 m*M* Tris–HCl buffer pH 6.5) and 1 µl reservoir solution. Red crystals grew to dimensions of 0.6 × 0.4 × 0.05 mm within one week over a reservoir solution consisting of 0.1 *M* MES pH 6.5, 2.1 *M* ammonium sulfate. For cryoprotection, the crystals were transferred to a solution consisting of the reservoir solution supplemented with 30%(*v*/*v*) glycerol.

For initial crystallization screenings, freshly isolated cyt c_{6C} was transferred to 10 m*M* Tris–HCl pH 7.5. Small red crystals were obtained in 18 of the 196 conditions tested. Several crystals from different conditions were harvested and used for data collection. Despite the low resolution of the data (∼3 Å), analysis of the Matthews coefficient (Matthews, 1968) revealed an unexpectedly low water content. SDS–PAGE and electrospray ionization mass-spectrometric analysis of dissolved crystals revealed that the protein had been degraded. Protein-stabilization studies suggested that the addition of NaCl to a final concentration of 0.15–0.2 *M* should effectively stabilize the protein. Therefore, for the next round of crystallization screening at the HTX facility at EMBL Hamburg, cyt c_{6C} and its L50Q mutant were suspended in 10 m*M* Tris–HCl pH 7.5 with 0.2 *M* NaCl. The screening included the The Classics, Classics II, PACT and AmSO4 Suites (Qiagen). The sitting-drop vapour-diffusion technique was used at 292 K by mixing 0.2 µl protein solution (1 m*M* in 10 m*M* Tris buffer pH 7.5, 0.2 *M* NaCl) and 0.2 µl reservoir solution. Optimization of the crystallization conditions was carried out using the hanging-drop vapour-diffusion method at 292 K by mixing 1 µl protein solution and 1 µl reservoir solution. Red crystals (0.4 × 0.4 × 0.2 mm) suitable for X-ray analysis were obtained from 1.7 *M* NaCl, 2 *M* ammonium sulfate over a period of one week. For cryoprotection, the crystals were transferred to a solution consisting of the reservoir solution supplemented with 5 *M* NaCl. Interestingly, initial cryoprotection trials using the reservoir solution supplemented with 30% glycerol resulted in much poorer diffraction (1.6 Å).

2.5. X-ray data collection

X-ray diffraction data were collected at 100 K on the X11 and X13 synchrotron beamlines at the EMBL Outstation, c/o DESY, Hamburg. Integration, scaling and merging of the intensity data was accomplished with the *XDS* package (Kabsch, 2010) for the cyt c_6, Q57V c_6 and L50Q c_{6C} data and with *MOSFLM*/*SCALA* (Leslie & Powell, 2007; Evans, 2006) for the cyt c_{6C} data. Space groups, unit-cell parameters and data-collection statistics are given in Table 1.

Data measured to high resolution using synchrotron radiation can be affected by radiation damage. However, a plot of the decay *R* factor (Diederichs, 2006) against the frame number indicated a value of close to zero and the scaling factors of the individual diffraction images fluctuated around 1 without any decreasing trend, indicating no or little influence of radiation damage. The data were also checked for diffraction anisotropy (Strong *et al.*, 2006), but a very low spread in the values of the three principal components (0.85, 2.18, 1.67 and 1.47 Å^2 for the cyt c_6, Q57V c_6, c_{6C} and L50Q c_{6C} data, respectively) indicated almost no anisotropy.

2.6. Structure solution and refinement

2.6.1. Cytochrome c_6. The structure of cyt c_6 was solved by molecular replacement using *MOLREP* from the *CCP*4 suite (Vagin & Teplyakov, 2010; Winn *et al.*, 2011) and the structure of the same protein in another crystal form (PDB entry 3dr0; Bialek *et al.*, 2009) as the search model. The initial maximum-likelihood structure-factor refinement was carried out in *REFMAC*5 (Murshudov *et al.*, 2011) using all intensity data, with the exception of 974 reflections that were flagged for cross-validation purposes. No σ-cutoff was applied. The manual rebuilding of the model was performed in *Coot* (Emsley & Cowtan, 2004). The conjugate-gradient least-squares (CGLS) procedure of *SHELXL* (Sheldrick, 2008) was used to refine the model in the later stages. The main steps of the refinement included (i) isotropic refinement with manually added water and MES molecules, (ii) anisotropic refinement, (iii) addition of riding H atoms according to the geometrical criteria implemented in *SHELXL*, (iv) refinement of the occupancies of partially occupied/alternate conformations and solvent atoms and finally (v) removal of the restraints for the well ordered parts of the model. Six side chains, namely Val25, Tyr39, Lys44, Glu51, Pro66 and Arg71, were modelled with alternate conformations. Additionally, the last four atoms of Gln8 and Asp45, the last three atoms of Met26 and Lys92, and the last two atoms of Lys44 were refined with partial occupancies. Stereochemical restraints were retained throughout all refinement only for these side chains.

In the final round, all data were used in the refinement, including the $R_{\rm free}$ reflections, leading to convergence with *R* values of 9.54% for the 54 437 reflections with $F_{\rm o} > 4\sigma(F_{\rm o})$ and 10.58% for all 64 908 reflections (Table 1).

At the end of the refinement, one cycle of full-matrix minimization was performed with all stereochemical restraints removed and with all parameter shifts damped to zero, which

Table 1
Data-collection and refinement statistics.

Values in parentheses are for the highest resolution shell.

PDB code	4eic	4eid	4eie	4eif
Data collection				
Space group	$P2_1$	$P2_1$	$P42_12$	$P42_12$
Unit-cell parameters (Å, °)	a = 31.86, b = 27.69, c = 44.07, β = 101.10	a = 31.78, b = 27.64, c = 44.10, β = 101.16	a = b = 56.13, c = 44.07	a = b = 56.38, c = 50.05
X-ray source	X11, EMBL/DESY	X11, EMBL/DESY	X11, EMBL/DESY	X13, EMBL/DESY
Wavelength (Å)	0.8166	0.8150	0.8149	0.8123
Temperature (K)	100	100	100	100
Mosaicity (°)	0.25	0.34	0.46	0.22
Resolution range (Å)	35.0–0.84 (0.86–0.84)	50.0–1.13 (1.20–1.13)	25.0–1.03 (1.09–1.03)	50.0–1.04 (1.10–1.04)
$R_{\rm int}$† (%)	6.3 (50.7)	5.0 (45.1)	8.8 (83.2)	7.3 (24.4)
$\langle I/\sigma(I)\rangle$	15.2 (3.2)	15.3 (2.0)	21.8 (2.9)	22.3 (7.8)
Reflections (measured/unique)	389855/64908	91869/28144	925352/39532	405268/39071
Multiplicity	6.0 (4.3)	3.3 (1.7)	23.4 (13.5)	10.4 (7.6)
Completeness (%)	94.8 (80.6)	99.1 (96.8)	99.3 (100.0)	99.2 (98.7)
Wilson B factor (Å^2)	9.45	13.32	8.00	10.13
Refinement				
Refinement program	*SHELXL*	*REFMAC*	*REFMAC*	*REFMAC*
Resolution range (Å)	32.50–0.84	43.30–1.13	19.84–1.03	31.18–1.04
No. of reflections				
Working set	63934	27159	38488	39071
Test set	974	986	1017	977
$R_{\rm work}/R_{\rm free}$‡ (%)	10.6/12.7	13.8/17.6	13.6/16.2	11.9/14.5
No. of atoms				
Protein	705	703	664	665
Solvent	120	152	134	147
$\langle B\rangle$ (Å^2)				
Protein	8.54	9.03	11.56	8.92
Solvent	16.83	18.35	21.60	18.44
R.m.s. deviations from ideal				
Bond lengths (Å)	0.026	0.023	0.021	0.019
Bond angles (°)		1.87	1.87	1.85
Angle distances (Å)	0.034			
Ramachandran statistics (%)				
Favoured	96.7	96.7	97.6	97.7
Additionally allowed	3.3	3.3	2.4	2.3

† $R_{\rm int} = \sum_{hkl}\sum_i |I_i(hkl) - \langle I(hkl)\rangle| / \sum_{hkl}\sum_i I_i(hkl)$, where $I_i(hkl)$ is the ith measurement of the intensity of reflection hkl and $\langle I(hkl)\rangle$ is the mean intensity of reflection hkl. ‡ $R = \sum_{hkl} ||F_{\rm obs}| - |F_{\rm calc}|| / \sum_{hkl} |F_{\rm obs}|$, where $|F_{\rm obs}|$ and $|F_{\rm calc}|$ are the observed and calculated structure factor-amplitudes, respectively. $R_{\rm free}$ is calculated analogously for the test reflections, which were randomly selected and excluded from the refinement.

permitted estimation of the standard uncertainties (s.u.s) in all positional parameters.

The final model contains one entire cytochrome c_6 molecule, 120 water molecules (six in alternative locations) and one MES molecule. The quality of the structure was assessed with *MolProbity* (Chen *et al.*, 2010). The final model is characterized by a root-mean-square deviation (r.m.s.d.) from ideal bond lengths of 0.026 Å, with 96.7% of all residues in the most favoured areas of the Ramachandran plot and with no residues in disallowed regions. The refinement statistics are reported in Table 1.

2.6.2. Q57V mutant of cytochrome c_6. The structure of Q57V cyt c_6 was solved by molecular replacement using the *MOLREP* program from the *CCP*4 suite and the structure of cyt c_6 as the search model. Maximum-likelihood structure-factor refinement was carried out in *REFMAC*5 using all intensity data, with the exception of 986 reflections that were flagged for cross-validation purposes. No σ-cutoff was applied. Manual rebuilding of the model was performed in *Coot*.

In the final stages the model was refined with anisotropic atomic displacement parameters and with H atoms added at riding positions. The final model contains one entire Q57V c_6 molecule, 140 water molecules (ten in alternative locations) and one MES molecule. The quality of the structure was assessed with *MolProbity*. The refinement converged with a final R factor of 13.8% ($R_{\rm free}$ = 17.6%). The final model is characterized by an r.m.s.d. from ideal bond lengths of 0.023 Å, with 96.7% of all residues in the most favoured areas of the Ramachandran plot and with no residues in disallowed regions. The refinement statistics are given in Table 1.

2.6.3. Cytochrome c_{6C}. Despite 40.7% sequence identity and 64.9% sequence similarity to cyt c_6, it was not possible to solve the crystal structure of cyt c_{6C} by molecular replacement using either *MOLREP* or *Phaser* (McCoy *et al.*, 2007). The structure of cyt c_{6C} was solved using the anomalous scattering of iron and the SAD protocol of *Auto-Rickshaw* (Panjikar *et al.*, 2005, 2009) in space group $P42_12$. The input diffraction data were converted to *Auto-Rickshaw* format using programs from the *CCP*4 suite (Winn *et al.*, 2011). ΔF(ano) values were calculated in *SHELXC* (Sheldrick *et al.*, 2001). Based on an initial analysis of the data, the maximum resolution for substructure determination and initial phase calculation was set to 1.6 Å. One Fe position was located using *SHELXD* (Schneider & Sheldrick, 2002). The correct hand of the

substructure was determined using *ABS* (Hao, 2004) and *SHELXE* (Sheldrick, 2002). Initial phases were calculated after density modification using *SHELXE*. 90.4% of the model was built using *ARP*/*wARP* (Perrakis *et al.*, 1999). The resulting model was used as a starting model in the *MRSAD* protocol of *Auto-Rickshaw* for phase improvement. Initial refinement of the model using *REFMAC*5 resulted in an R factor of 35% and an $R_{\rm free}$ of 37%. Phasing was continued using *Phaser* and the partial model plus the heavy-atom position. The resulting phases were subjected to density modification using the program *Pirate* (Winn *et al.*, 2011) to the maximum resolution of 1.15 Å. This allowed *ARP*/*wARP* to build 75 residues (out of 87) as a single chain and most of the sequence was docked correctly. *REFMAC* refinement of this model resulted in R = 28.2% and $R_{\rm free}$ = 29.6%.

The subsequent maximum-likelihood structure-factor refinement was carried out in *REFMAC*5 using all intensity data, with the exception of 1017 reflections that were flagged for cross-validation purposes. No σ-cutoff was applied. Manual rebuilding of the model was performed in *Coot*. In the final stages the model was refined with anisotropic atomic displacement parameters and with H atoms added at riding positions. The final model contains one cyt c_{6C} molecule from Asp4 to Trp85 (two amino acids are missing at the C-terminus), 126 water molecules (five in alternative locations), four chloride anions and four sodium cations. The quality of the final structure was assessed with *MolProbity*. The refinement converged with an R factor of 13.6% and an $R_{\rm free}$ of 16.2%. The final model was characterized by an r.m.s.d. from ideal bond lengths of 0.021 Å, with 97.6% of all residues in the most favoured areas of the Ramachandran plot and with no residues in disallowed regions. The refinement statistics are reported in Table 1.

2.6.4. L50Q cytochrome c_{6C}. The structure of L50Q cyt c_{6C} was solved by molecular replacement using *MOLREP* from the *CCP*4 suite and the structure of the cyt c_{6C} protein as the search model. The initial maximum-likelihood structure-factor refinement was carried out in *REFMAC*5 using all intensity data, with the exception of 977 reflections that were flagged for cross-validation purposes. No σ-cutoff was applied. To account for diffuse solvent effects, a correction according to the Babinet principle was applied (Moews & Kretsinger, 1975). Manual rebuilding of the model was performed in *Coot*.

In the final stages the model was refined with anisotropic atomic displacement parameters and with H atoms added at riding positions. The final model consists of one L50Q cyt c_{6C} molecule of the same length as cyt c_{6C}, 140 water molecules (four in alternative locations), four chloride anions and three sodium cations. The quality of the final structure was assessed with *MolProbity*. The refinement converged with an R factor of 11.9% ($R_{\rm free}$ = 14.5%). The final model is characterized by an r.m.s.d. from ideal bond lengths of 0.019 Å, with 97.7% of all residues in the most favoured areas of the Ramachandran plot and with no residues in disallowed regions. The refinement statistics are reported in Table 1.

3. Results and discussion

3.1. Structure description

Overall, the structure of *Synechococcus* sp. PCC 7002 cyt c_{6C} reveals the characteristic properties of other class I cytochromes c (Fig. 1). A single polypeptide chain wraps around the haem moiety. The polypeptide chain consists of four α-helices connected by loops. The long N-terminal helix I (Gln5–His18) has a characteristic kink at Cys14 as in classical cyt c_6. The two cysteine residues forming the covalent links to the haem group (Cys14 and Cys17) and the fifth iron-coordinating ligand, His18, are part of this helix. As in cyt c_6 molecules, three consecutive amino-acid residues, Leu19–Gly21, form a 3_{10}-helix followed by the Ω-loop spanning residues Gly22–Leu31. Two Asx turns of type II′ (Asn23–Val25) and I (Asn30–Lys32) are present inside this Ω-loop. The Ω-loop separates helix I from the short helix II (Lys33–Asn39). At the C-terminus of helix II, there is a right-handed Schellman loop/paperclip motif (Met36–Tyr41) with an RL nest at the i + 4 position. In the relatively long region between helix III (Val44–Gln53) and helix IV there are three β-turns of types II′ (Lys55–Met58), I (Tyr61–Lys64) and IV (Gly62–Leu65). The longest helix IV, which is nearly perpendicular to helix I, runs from Ser67 to Gln82. In the described model of cyt c_{6C} no salt bridges are found.

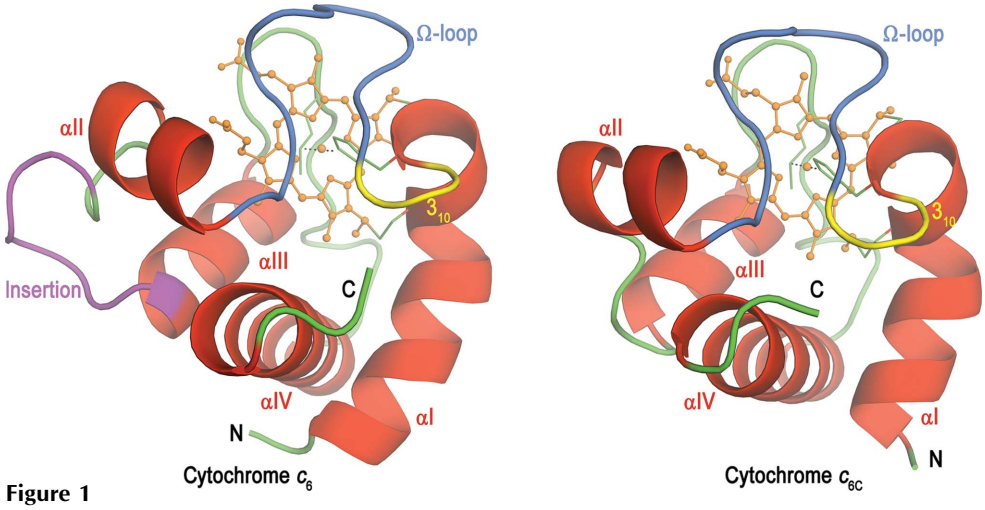

Figure 1
Overall architecture of cyt c_6 and c_{6C}. The secondary structure of both cytochromes includes α-helices (red), a 3_{10}-helix (yellow) and several loops (green). The Ω-loop characteristic of cytochromes c is indicated in cyan and the unique insertion of cyt c_6 from *Synechococcus* sp. PCC 7002 is highlighted in magenta. The haem group is shown in orange ball-and-stick representation.

The structure of cyt c_6 from *Synechococcus* sp. PCC 7002 was refined to ultrahigh resolution. By changing the buffering conditions (§2), cyt c_6 crystallized in a new crystal form. Unlike the previously described crystals of cyt c_6 (Bialek *et al.*, 2009), which belonged to space group $P3_2$ and diffracted X-rays to 1.23 Å resolution, the new crystals belonged to space group $P2_1$ and diffracted X-rays to the ultrahigh resolution of 0.84 Å. In addition, the $P2_1$ asymmetric unit contains one protein molecule as opposed to the three molecules found in the $P3_2$ crystal form (PDB entry 3dr0). Whereas the mean C^{α} r.m.s.d. value for the three independent molecules in the former structure is 0.33 Å, this value is 0.5 Å for comparisons with the present model. The largest deviation is observed at Asp45 and Gly46 inside a loop unique to known cyts c_6. The function of this loop has not yet been established, although a mutant with a deletion of this loop has a significantly lower midpoint potential (E_m = 235.8 mV) than the wild-type (WT) protein. This may suggest that removal of this loop leads to conformational changes that influence the midpoint potential (P. Zatwarnicki, unpublished work).

As expected, the mutation of one residue within the haem pocket does not significantly affect the tertiary structure. The superposition of WT and Q57V cyt c_6 using the *SSM* algorithm implemented in *Coot* (Emsley & Cowtan, 2004) gave an r.m.s.d. of 0.10 Å, with the largest difference of 0.22 Å for the C^{α} atoms of Tyr56. Also, conformations of the side chains that are not adjacent to the haem pocket are similar.

3.2. Haem environment

The overall fold of cyt c_{6C} is typical of cyt *c* proteins, *i.e.* the porphyrin moiety is slightly distorted into a saddle shape and the haem is covalently linked to the polypeptide chain through two thioether bonds from the Cys14 and Cys17 sulfhydryl groups located inside the hydrophobic pocket. The iron ion is coordinated through the His18 $N^{\varepsilon 2}$ and Met58 S^{δ} atoms located at axial positions. The distances from the haem iron to His18 $N^{\varepsilon 2}$ and to Met58 S^{δ} are 1.99 and 2.34 Å, respectively, and the $N^{\varepsilon 2}$—Fe—S^{δ} angle is 176.2°. In the cyt c_6 from the cyanobacterium studied here, as well as in the cyt c_6 and cyt c_{6C} point mutants, the corresponding bond distances and angles are almost identical. As in classical cyt c_6 proteins, a hydrogen bond between the $N^{\delta 1}$—H donor of the axial His18 and a main-chain carbonyl O atom of a residue from the 3_{10}-helix (Gly22 in the case of c_{6C} and Asn22 in c_6) serves to maintain the required orientation of the His ring with respect to the haem plane, whereas the O and N atoms of Met58 are hydrogen-bonded to the backbone atoms of Lys55, forming a II′ turn (Lys55–Met58).

A total of three water molecules are present within hydrogen-bonding distance around the haem-propionate side chains in both wild-type structures (W201, W215 and W268 in cyt c_6 and W207, W255 and W303 in cyt c_{6C}). In cyt c_6 the water molecule W201 forms a hydrogen-bond bridge between the haem propionates. This water molecule also interacts with the N^{ε} atom of Gln57 and W202. The haem-6-propionate forms hydrogen bonds to the N^{ζ} atom of Lys29 and water W268, which is in turn hydrogen-bonded to N^{ε} of Gln62. A third water molecule, W215, forms a bridge between the haem-6-propionate and the N atom of Ala64. Additionally, the haem-7-propionate makes hydrogen-bond contacts with the O atom of Thr30.

In the Q57V c_6 mutant, there is also a water molecule (W260) in the haem-binding pocket that connects the haem-6-propionate and Glu62. As in wild-type cyt c_6, another water molecule (W216) interconnects the haem-6-propionate with the N atom of Ala64. Moreover, there is a water molecule that interacts with both propionates (W309). Because of the absence of the glutamine polar side chain in the Q57V mutant, the nature of the hydrogen-bonding interactions is different.

In cyt c_{6C}, the haem-6-propionate is also hydrogen-bonded to three water molecules: W207, W255 and W303. W255 further interacts with haem-7-propionate and W244, W207 further interacts with the N atom of Asn57, W325 and Cl102, and W303 further interacts with N^{ζ} of Lys29. On the other hand, the haem-7-propionate makes hydrogen-bond contacts with the main-chain O atom of Asn30 and $N^{\delta 2}$ of Asn39 (from a minor conformer).

In the L50Q cyt c_{6C} structure only two water molecules (W219 and W293) directly interact with the haem-6-propionate, forming hydrogen-bond contacts to N^{ε} of Gln50 (W293) and to the N atom of Asn57, W304 and Cl105 (W219). Furthermore, the haem-6-propionate is directly bonded to N^{ζ} of Lys29 and $N^{\eta 1}$ of Arg26 (only one conformer of the two modelled is involved in these interactions; Fig. 2).

Although in both cyt c_6 and c_{6C} the haem moiety is surrounded by amino-acid residues and structural water molecules involved in mutual hydrogen bonds, the pattern of these interactions is different. Owing to the presence of two polar residues, Gln57 and Gln62, in the cyt c_6 haem crevice, there are two structural water molecules (W201 and W268) interacting with these residues and both haem-propionates. Because there are no polar residues in adequate positions in cyt c_{6C}, these structural waters are missing.

Our calculations of haem exposure to solvent reveal that the haem group of cyt c_{6C} is as exposed as that of cyt c_6. The total solvent-exposed areas are 65.2 and 61.4 $Å^2$, respectively.

3.3. Reduction potentials and spectroscopic features

As shown in Fig. 3 and Table 2, the UV–Vis absorption spectra of purified cytochrome c_6 from *Synechococcus* sp. PCC 7002 in its oxidized and reduced states are similar to the spectra of cytochromes c_6 from other species, with a characteristic α-band at 553.2 nm. In contrast, in the case of c_{6C} cytochrome the absorbance maxima of the α, β and Soret bands are red-shifted in the reduced protein. Interestingly, for Q57V cyt c_6 two shoulders next to the α and β reduced bands are clearly visible even though the spectra were taken at room temperature. Split or asymmetric bands in the visible region are observed at 77 K and have been recorded for many cytochromes (Sherman *et al.*, 1991; Reddy *et al.*, 1996). Similar to cyt c_6 from *Phormidium laminosum*, substitution of the conserved glutamine residue by valine in cyt c_6 from *Syne-*

chococcus sp. PCC 7002 resulted in a bathochromic shift of the reduced α band. By contrast, substitution of leucine by glutamine caused a hypsochromic shift in cyt c_{6C} (Fig. 3).

More importantly, we confirmed our previous findings regarding differences in redox midpoint potential (Fig. 4). While c_6, with an E_m of +333 $\pm$ 4.6 mV, is a typical high-potential protein, the E_m of cyt c_{6C} is less than half of this value (+155 $\pm$ 5.8 mV). These measurements agree with our first redox titrations (Bialek *et al.*, 2008). However, site-specific mutations of a single conserved residue inside the haem pocket result in drastic changes. As in the case of cyt c_6 from *P. laminosum* (Worrall *et al.*, 2007), mutation of the absolutely conserved glutamine residue of cyt c_6, *e.g.* Q57V in the case of *Synechococcus* sp. PCC 7002, lowers the redox potential of the whole protein to +240 $\pm$ 2.4 mV. By analogy, substitution of the corresponding residue in cytochrome c_6-like proteins, which in these proteins is always an aliphatic residue (valine, leucine or isoleucine), by a polar residue

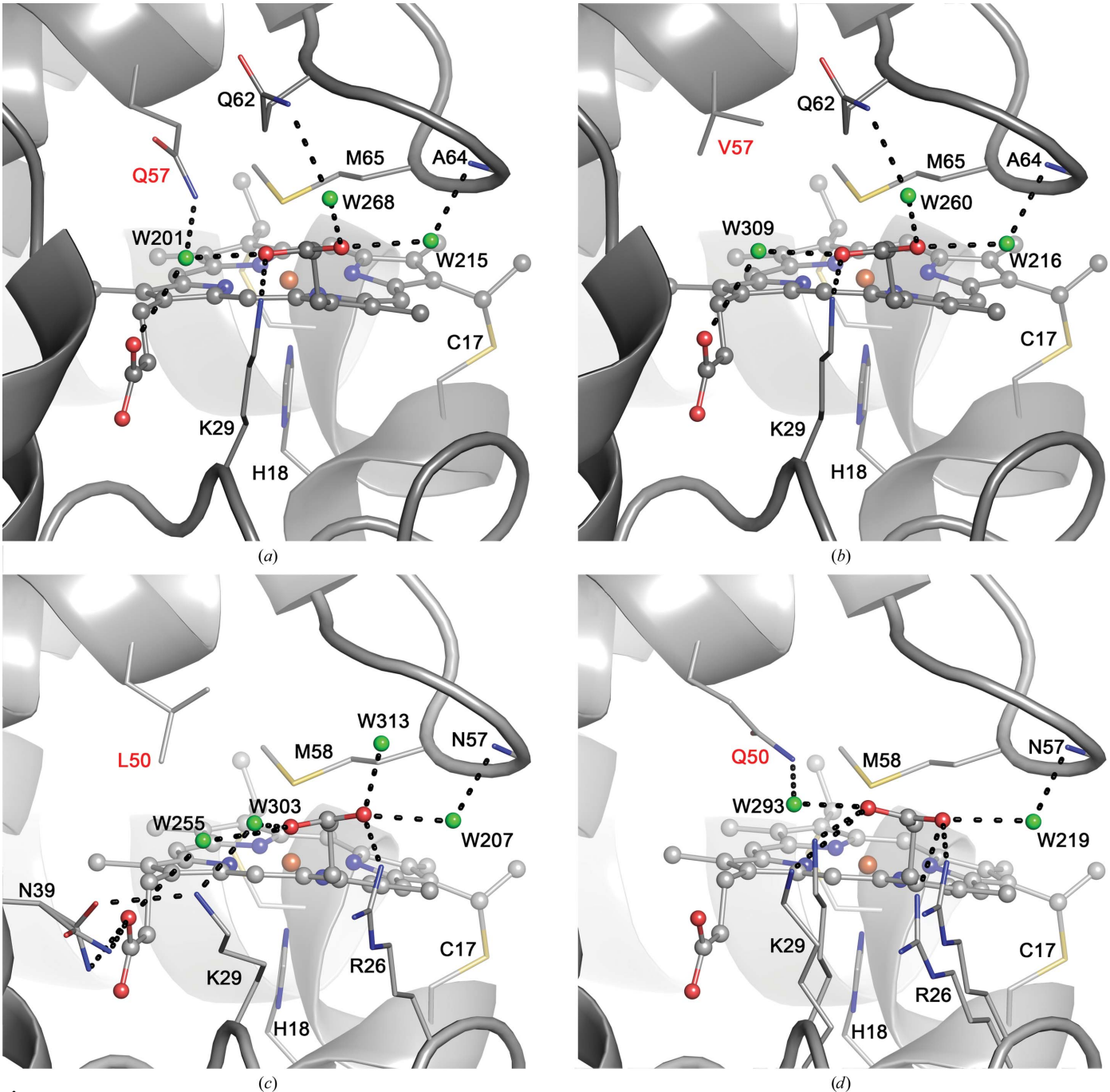

Figure 2
Haem pockets of wild-type cyt c_6 (*a*) and Q57V cyt c_6 (*b*) (dark grey) and wild-type cyt c_{6C} (*c*) and L50Q c_{6C} (*d*) (light grey) from *Synechococcus* sp. PCC 7002. The positions of mutated residues are shown in red. Asn39 (*c*) and Arg26 and Lys29 (*d*) are shown as two possible conformers fitted to the electron density. Water molecules and haem irons are depicted as green and orange spheres, respectively. The occupancy factor for W303 and W313 (*c*) is 0.5. Dashed lines represent hydrogen bonds.

(glutamine) results in an increase in E_m. Here, we show that the substitution of leucine by glutamine (L50Q) increases the E_m of cyt c_{6C} to 203 ± 3.0 mV, similar to c_{6A} from *A. thaliana*, in which a valine-to-glutamine substitution also increases E_m (Worrall *et al.*, 2007). In summary, the decrease of the midpoint potential by 93 mV in cyt c_6 from *Synechococcus* sp. PCC 7002 is similar to the effects of an identical mutation in cyt c_6 from *P. laminosum* (Rajagopal *et al.*, 2011). Thus, glutamine-to-valine substitution results in a drastic decrease in E_m and accounts for about half of the difference between c_6 and c_{6C}. On the other hand, an analogous substitution of leucine by glutamine increases the potential of cyt c_{6C} by almost 50 mV, but the mutation of valine to glutamine in another cyt c_6-like protein, cyt c_{6A} from *A. thaliana*, increased the E_m more significantly by 103 mV (Worrall *et al.*, 2007). This discrepancy may result from differences within the haem pocket, such as different numbers of structural water molecules (three and two in cyt c_{6C} and c_{6A}, respectively) and different hydrogen-bond networks.

3.4. Electrostatic properties

To elucidate the possible role of the protein electrostatic surface potential responsible for cytochrome function, we compared surface-potential maps of several cyt c_6 molecules with cyt c_{6C}, as shown in Fig. 5. Generally, a similar charge distribution is observed for cyt c_6, with a conserved so-called north face (Molina-Heredia *et al.*, 1999). Typically, on the north face a hydrophobic area surrounds the haem crevice, whereas the east face of cyt c_6 is decorated with positive charges. Not surprisingly, the area around the haem crevice is used as the site for recognition during electron transfer, whereas the east face is involved in long-range electrostatic interactions with cyt partners. Importantly, the charge distribution differs drastically between cyt c_6 and c_{6C} from *Synechococcus* sp. PCC 7002, which agrees with their very acidic and basic pI values, respectively. The most important difference lies in the east face, which is heavily negatively charged in cyt c_{6C}. As this is the only available structure of cyt c_{6C} to date, there are no other available data about surface charge distribution in proteins of this type apart from the theoretical calculations of Reyes-Sosa *et al.* (2011). Their data suggest that other cyt c_6-like proteins from nitrogen-fixing cyanobacteria have a similar negative patch.

In addition, we found another significant difference between cyt c_6 and c_{6C} in the vectors of the dipole moments. Although the vectors are similarly oriented, the overall molecular dipole moments are strikingly different. As esti-

Table 2
Comparison of the absorbance maxima (nm) of the α, β and Soret (γ) bands for the reduced cytochromes c_6 and c_{6C} as well as for their point mutants.

	Peak		
Cytochrome	α	β	γ
cyt c_6	553.2	522.4	416.5
cyt c_6 Q57V	555.9	522.5	417.6
cyt c_{6C}	556.1	523.8	416.5
cyt c_{6C} L50Q	553.5	522.7	415.4

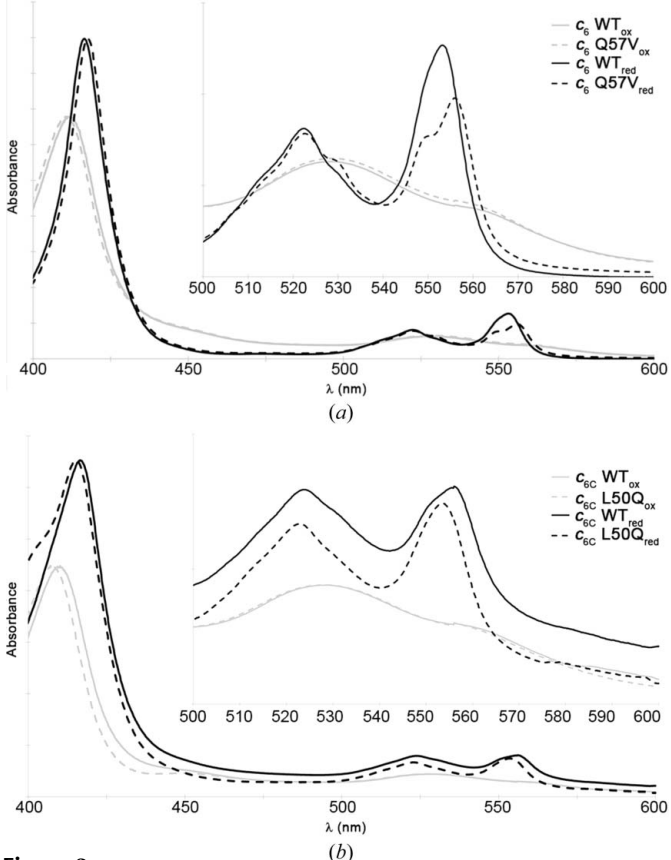

Figure 3
Absorbance spectra of wild-type (continuous line) and mutated (dashed line) cyt c_6 (*a*) and cyt c_{6C} (*b*). The spectra of oxidized (ox) and reduced (red) cyts were normalized to the Soret bands.

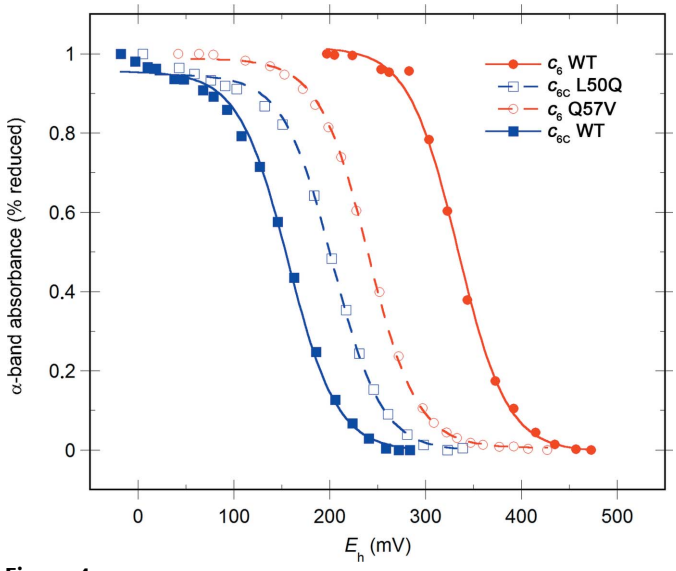

Figure 4
Potentiometric redox titrations of WT and Q57V cyts c_6 (red open and closed circles, respectively) and WT and L50Q cyts c_{6C} (blue open and closed squares, respectively). Titrations were conducted three times in the oxidative and reductive directions. The curves were fitted to single-electron Nernst equations.

mated using the *Protein Dipole Moments Server* (http://dipole.weizmann.ac.il/), the molecular dipole moment of cyt c_{6C} is 503 D, *i.e.* it is 2.6–2.9 times higher than that for c_6 (193 D for the present model and 175 D in the case of structure 3dr0) from the same cyanobacterium. The unusual surface charge distribution noted above leads to a very strong dipole, which may be involved in docking cyt c_{6C} in position for electron transfer. Together, these results enable us to identify putative 'hot spots' in cyt c_{6C}, as electrostatic interactions play a more important role in protein binding than they do in folding.

3.5. c_6-like proteins of *Synechococcus* sp. PCC 7002 and *Nostoc* sp. PCC 7119

Recently, a cyt c_6-like protein from *Nostoc* sp. PCC 7119 was characterized to some extent by Reyes-Sosa *et al.* (2011). Using the sequence provided in the publication, we were able to identify this protein as a cytochrome belonging to the same family as cyt c_{6C} from *Synechococcus* sp. PCC 7002. The proteins are 59% identical and 76% similar in terms of their primary structure. Thus, cyt c_{6C} is less similar to cyt c_6 from the same species, *Synechococcus* sp. PCC 7002 (40% identical and 57% similar), than it is to cyt c_{6C} from a relatively distant cyanobacterium. *Nostoc* sp. PCC 7119 is a filamentous, heterocystous nitrogen-fixing cyanobacterium, whereas *Synechococcus* sp. PCC 7002 represents a marine cyanobacterium. In addition, the estimated $E_{m,7}$ for cyt c_{6C} from *Nostoc* sp. PCC 7119 is the second to be reported for this group of cyt c_6-like proteins and is +199 mV. It is 51 mV higher than the value reported here for the first identified c_{6C} protein from *Synechococcus* sp. PCC 7002. However, similar differences are observed in the case of all cyt c_6 proteins, for instance the $E_{m,7}$ values for cyt c_6 from *Synechococcus* sp. PCC 7002 and *A. maxima* are 319 and 314 mV, respectively (Bialek *et al.*, 2008; Cho *et al.*, 1999) and those for *C. reinhardtii* and *C. fusca* are 370 and 360 mV, respectively (Gorman & Levine, 1966; Inda *et al.*, 1997). On the other hand, both cyt c_{6C} proteins characterized so far are basic proteins.

The amino-acid sequences of cyt c_6 and cyt c_{6C} from *Synechococcus* sp. PCC 7002 are 40% identical. We have resolved the structure of cyt c_6 from this cyanobacterium before (Bialek *et al.*, 2009) and we now compare the structural features of the two proteins. Currently, the structures of many *c*-type cytochrome proteins are available. The structure most similar to cyt c_{6C} is indeed that of cyt c_6, although structural alignment suggested that the most similar protein structure would correspond to cyt c_6 from another cyanobacterium, *P. laminosum*, with an r.m.s.d. of 0.58 Å. The average r.m.s.d. and sequence identity for cyt c_6 and cyt c_{6A} are 0.59 Å and 44%, respectively. Interestingly, the lowest level of similarity to c_{6C} is shown by cytochrome c_6 from *Synechococcus* sp. PCC 7002. Using the *Q*-value, which takes into account both r.m.s.d. and sequence identity, even OmcF from *G. sulfurreducens*, a δ-proteobacterium harbouring

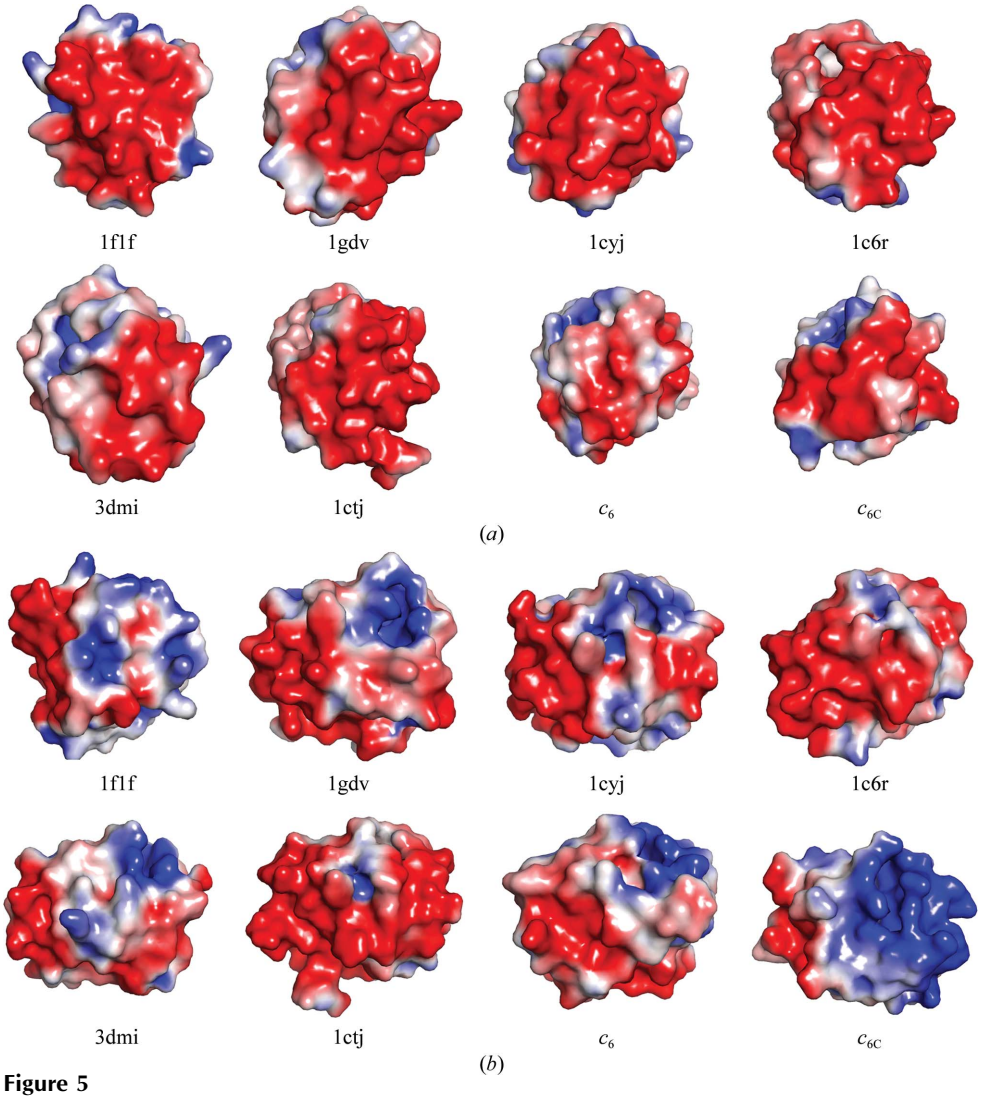

Figure 5
Comparison of surface-potential distributions of the north (*a*) and east (*b*) faces of cytochromes from *Arthrospira maxima* (PDB entry 1f1f; Sawaya *et al.*, 2001), *Porphyra yezoensis* (PDB entry 1gdv; Yamada *et al.*, 2000), *Chlamydomonas reinhardtii* (PDB entry 1cyj; Kerfeld *et al.*, 1995), *Chlorolobion braunii* (PDB entry 1ctj; Frazão *et al.*, 1995), *Scenedesmus obliquus* (PDB entry 1c6r; Schnackenberg *et al.*, 1999), *Phaeodactylum tricornutum* (PDB entry 3dmi; Akazaki *et al.*, 2009) and *Synechococcus* sp. PCC 7002 (c_6 and c_{6C}; this work).

more than 100 genes encoding various cytochrome *c*-type proteins, was found to be more similar to c_{6C} than cyt c_6 from *Synechococcus* sp. PCC 7002. Significantly lower levels of similarity were also found in relation to membrane-bound proteins, such as the cytochrome subunit of flavocytochrome *c* sulfide dehydrogenase from *Thioalkalivibrio nitratireducens* and *p*-cresol methylhydroxylase from *Pseudomonas aeruginosa*, as well as to different cytochromes: c_{553}, c_{552}, c_{551} and c_5.

The functions of both cyanobacterial and plant cyt c_6-like proteins remain unknown. However, the results presented here show that a similar trend exists between the plant cyt c_{6A} and cyt c_6 and the cyanobacterial cyt c_{6C} and cyt c_6 pairs. According to the hypothesis of Worrall *et al.* (2007), we have shown that in the case of cyt c_{6C} a single amino-acid substitution within the haem pocket also alters the most important biophysical property of a cytochrome, *i.e.* its redox potential.

This work was funded in part by grants N N303 817640 and N N204 245635 from the Ministry of Science and Higher Education. We would like to thank Dr Santosh Panjikar for help with *Auto-Rickshaw*.

References

Akazaki, H., Kawai, F., Chida, H., Matsumoto, Y., Hirayama, M., Hoshikawa, K., Unzai, S., Hakamata, W., Nishio, T., Park, S.-Y. & Oku, T. (2008). *Acta Cryst.* F**64**, 674–680.

Akazaki, H., Kawai, F., Hosokawa, M., Hama, T., Chida, H., Hirano, T., Lim, B.-K., Sakurai, N., Hakamata, W., Park, S.-Y., Nishio, T. & Oku, T. (2009). *Biosci. Biotechnol. Biochem.* **73**, 189–191.

Arslan, E., Schulz, H., Zufferey, R., Künzler, P. & Thöny-Meyer, L. (1998). *Biochem. Biophys. Res. Commun.* **251**, 744–747.

Beissinger, M., Sticht, H., Sutter, M., Ejchart, A., Haehnel, W. & Rösch, P. (1998). *EMBO J.* **17**, 27–36.

Bialek, W., Krzywda, S., Jaskolski, M. & Szczepaniak, A. (2009). *FEBS J.* **276**, 4426–4436.

Bialek, W., Nelson, M., Tamiola, K., Kallas, T. & Szczepaniak, A. (2008). *Biochemistry*, **47**, 5515–5522.

Braun, M. & Thöny-Meyer, L. (2004). *Proc. Natl Acad. Sci. USA*, **101**, 12830–12835.

Chen, V. B., Arendall, W. B., Headd, J. J., Keedy, D. A., Immormino, R. M., Kapral, G. J., Murray, L. W., Richardson, J. S. & Richardson, D. C. (2010). *Acta Cryst.* D**66**, 12–21.

Chida, H., Yokoyama, T., Kawai, F., Nakazawa, A., Akazaki, H., Takayama, Y., Hirano, T., Suruga, K., Satoh, T., Yamada, S., Kawachi, R., Unzai, S., Nishio, T., Park, S.-Y. & Oku, T. (2006). *FEBS Lett.* **580**, 3763–3768.

Cho, Y. S., Wang, Q. J., Krogmann, D. & Whitmarsh, J. (1999). *Biochim. Biophys. Acta*, **1413**, 92–97.

Diederichs, K. (2006). *Acta Cryst.* D**62**, 96–101.

Dikiy, A., Carpentier, W., Vandenberghe, I., Borsari, M., Safarov, N., Dikaya, E., Van Beeumen, J. & Ciurli, S. (2002). *Biochemistry*, **41**, 14689–14699.

Dutton, P. L. (1978). *Methods Enzymol.* **54**, 411–435.

Emsley, P. & Cowtan, K. (2004). *Acta Cryst.* D**60**, 2126–2132.

Evans, P. (2006). *Acta Cryst.* D**62**, 72–82.

Frazão, C., Dias, J. M., Matias, P. M., Romão, M. J., Carrondo, M. A., Hervás, M., Navarro, J. A., De La Rosa, M. & Sheldrick, G. M. (1995). *Acta Cryst.* D**51**, 232–234.

Gorman, D. S. & Levine, R. P. (1966). *Plant Physiol.* **41**, 1643–1647.

Hao, Q. (2004). *J. Appl. Cryst.* **37**, 498–499.

Inda, L. A., Medina, M., Saraiva, L. M. & Gómez-Moreno, C. (1997). *Photosynth. Res.* **54**, 107–114.

Jancarik, J. & Kim, S.-H. (1991). *J. Appl. Cryst.* **24**, 409–411.

Kabsch, W. (2010). *Acta Cryst.* D**66**, 125–132.

Kerfeld, C. A., Anwar, H. P., Interrante, R., Merchant, S. & Yeates, T. O. (1995). *J. Mol. Biol.* **250**, 627–647.

Leslie, A. G. W. & Powell, H. R. (2007). *Evolving Methods for Macromolecular Crystallography*, edited by R. J. Read & J. L. Sussman, pp. 41–51. Dordrecht: Springer.

Lukat, P., Hoffmann, M. & Einsle, O. (2008). *Acta Cryst.* D**64**, 919–926.

Marcaida, M. J., Schlarb-Ridley, B. G., Worrall, J. A., Wastl, J., Evans, T. J., Bendall, D. S., Luisi, B. F. & Howe, C. J. (2006). *J. Mol. Biol.* **360**, 968–977.

Matthews, B. W. (1968). *J. Mol. Biol.* **33**, 491–497.

McCoy, A. J., Grosse-Kunstleve, R. W., Adams, P. D., Winn, M. D., Storoni, L. C. & Read, R. J. (2007). *J. Appl. Cryst.* **40**, 658–674.

Moews, P. C. & Kretsinger, R. H. (1975). *J. Mol. Biol.* **91**, 201–225.

Molina-Heredia, F. P., Díaz-Quintana, A., Hervás, M., Navarro, J. A. & De La Rosa, M. A. (1999). *J. Biol. Chem.* **274**, 33565–33570.

Murshudov, G. N., Skubák, P., Lebedev, A. A., Pannu, N. S., Steiner, R. A., Nicholls, R. A., Winn, M. D., Long, F. & Vagin, A. A. (2011). *Acta Cryst.* D**67**, 355–367.

Panjikar, S., Parthasarathy, V., Lamzin, V. S., Weiss, M. S. & Tucker, P. A. (2005). *Acta Cryst.* D**61**, 449–457.

Panjikar, S., Parthasarathy, V., Lamzin, V. S., Weiss, M. S. & Tucker, P. A. (2009). *Acta Cryst.* D**65**, 1089–1097.

Perrakis, A., Morris, R. & Lamzin, V. S. (1999). *Nature Struct. Biol.* **6**, 458–463.

Pokkuluri, P. R., Londer, Y. Y., Wood, S. J., Duke, N. E., Morgado, L., Salgueiro, C. A. & Schiffer, M. (2009). *Proteins*, **74**, 266–270.

Rajagopal, B. S., Wilson, M. T., Bendall, D. S., Howe, C. J. & Worrall, J. A. (2011). *J. Biol. Inorg. Chem.* **16**, 577–588.

Reddy, K. S., Angiolillo, P. J., Wright, W. W., Laberge, M. & Vanderkooi, J. M. (1996). *Biochemistry*, **35**, 12820–12830.

Reyes-Sosa, F. M., Gil-Martínez, J. & Molina-Heredia, F. P. (2011). *Photosynth. Res.* **110**, 61–72.

Sawaya, M. R., Krogmann, D. W., Serag, A., Ho, K. K., Yeates, T. O. & Kerfeld, C. A. (2001). *Biochemistry*, **40**, 9215–9225.

Schnackenberg, J., Than, M. E., Mann, K., Wiegand, G., Huber, R. & Reuter, W. (1999). *J. Mol. Biol.* **290**, 1019–1030.

Schneider, T. R. & Sheldrick, G. M. (2002). *Acta Cryst.* D**58**, 1772–1779.

Sheldrick, G. M. (2002). *Z. Kristallogr.* **217**, 644–650.

Sheldrick, G. M. (2008). *Acta Cryst.* A**64**, 112–122.

Sheldrick, G. M., Hauptman, H. A., Weeks, C. M., Miller, R. & Uson, I. (2001). *International Tables for Macromolecular Crystallography*, Vol. *F*, edited by M. G. Rossmann & E. Arnold, pp. 333–345. Dordrecht: Kluwer Academic Publishers.

Sherman, D., Kotake, S., Ishibe, N. & Copeland, R. A. (1991). *Proc. Natl Acad. Sci. USA*, **88**, 4265–4269.

Strong, M., Sawaya, M. R., Wang, S., Phillips, M., Cascio, D. & Eisenberg, D. (2006). *Proc. Natl Acad. Sci. USA*, **103**, 8060–8065.

Vagin, A. & Teplyakov, A. (2010). *Acta Cryst.* D**66**, 22–25.

Winn, M. D. *et al.* (2011). *Acta Cryst.* D**67**, 235–242.

Wooh, J. W., Kidd, R. D., Martin, J. L. & Kobe, B. (2003). *Acta Cryst.* D**59**, 769–772.

Worrall, J. A., Schlarb-Ridley, B. G., Reda, T., Marcaida, M. J., Moorlen, R. J., Wastl, J., Hirst, J., Bendall, D. S., Luisi, B. F. & Howe, C. J. (2007). *J. Am. Chem. Soc.* **129**, 9468–9475.

Yamada, S., Park, S.-Y., Shimizu, H., Koshizuka, Y., Kadokura, K., Satoh, T., Suruga, K., Ogawa, M., Isogai, Y., Nishio, T., Shiro, Y. & Oku, T. (2000). *Acta Cryst.* D**56**, 1577–1582.